

Semi analytical description of formation of galaxies and clusters of galaxies

M. Demiański^{1,2}, A.G. Doroshkevich³,

¹*Institute of Theoretical Physics, University of Warsaw, 00-681 Warsaw, Poland*

²*Department of Astronomy, Williams College, Williamstown, MA 01267, USA*

³*Astro Space Center of Lebedev Physical Institute of Russian Academy of Sciences, 117997 Moscow, Russia*

Accepted ..., Received ..., in original form

ABSTRACT

We apply the well known semi analytical model of formation of DM halos to discuss properties of the relaxed objects dominated by the DM component (such as the first and dSph galaxies and/or clusters of galaxies). This approach allows us to obtain a simple but more detailed description of evolution of the first galaxies. It reveals also links between the observed characteristics of the relaxed DM halos and the initial power spectrum of density perturbations. Results of our analysis of the observed properties of ~ 40 DM dominated galaxies and ~ 100 clusters of galaxies are consistent with the Λ CDM like power spectrum of initial perturbations down to the scale of $\sim 10kpc$. For the DM dominated objects the scaling relations are also discussed.

Key words: cosmology: early galaxies–reionization of the Universe–scaling relations–formation of DM halos and clusters of galaxies.

1 INTRODUCTION

The formation and evolution of the first galaxies at redshifts $z \geq 8$ is one of the most interesting problems of modern cosmology and it is closely connected with many other unresolved problems. Among others there are the secondary ionization of the Universe at redshifts $z_{ri} \simeq 10$ implied by the WMAP observations (Komatsu et al. 2011; Larson et al. 2011) and recently confirmed by the PLANCK mission (Ade 2013), the formation and evolution of stars with the primeval chemical composition, the matter enrichment by metals, evolution of observed galaxies at redshifts $z \geq 6$, the high redshifts observations of massive galaxies and super massive black holes and so on (see, e.g., Wiklind et al. 2008; Mancini et al. 2009; Ouchi 2009; Vestergaard 2009; Trenti et al. 2009, 2010; Kelly 2010; Haiman 2010; Schaerer & de Barros 2010; Gonzales et al. 2010, 2012; Shull et al. 2011; Bouwense et al. 2011; Oesch et al. 2013; Ellis et al. 2013; Barone–Nugent 2013; Salvadori et al. 2013; Wyithe et al. 2013).

It is specially interesting that observations of the farthest quasars and galaxies show that the reionization of the hydrogen fraction of the intergalactic matter had just been completed already at $z \sim 7 - 8$ while ionization of HeII occurred only at $z \sim 3$ (Jakobsen et al. 1994; Hogan et al. 1997; Smette et al. 2002; Fan et al. 2004, 2006; Furlanetto and Oh 2008; Trenti et al. 2009; Lehnert et al. 2010; Robertson et al. 2010). This means that at least at $z \sim 5 - 7$ the ultraviolet (UV) radiation with energy $h\nu \geq 50$ eV is weak and it is

mainly generated by quasars at $z \leq 4$. The current status of these problems is discussed in many recent reviews (see, e.g., Bromm & Yoshida 2011; Johnson 2011; Kravtsov & Borgani 2013).

It is very difficult to find or even estimate characteristics of the first galaxies formed from matter of the primordial chemical composition. The absence of metals makes cooling of matter and formation of stars more difficult and leads to well known peculiarities in the evolution of such objects. First of all it is the high typical mass of first stars ($100 - 1000 M_{\odot}$) and significant energy that they eject in the UV region and during the ultimate explosion as supernovae (see, e.g., Tumlinson et al. 2004; Trenti & Shull 2010; Bromm & Yoshida 2011). At the same time radiation of these stars generates the Lyman – Werner (LW) and infrared (IR) backgrounds that destroy the H^{-} ions and H_2 molecules what delays the cooling of matter and slows down the process of star formation.

Some observations (e.g., Bouwens et al. 2011) show that the observed rate of star formation and predicted UV radiation cannot ionize the Universe at $z \sim 10$. Alternative explanation assumes that properties of galaxies at small and high redshifts can be quite different (Ouchi et al. 2009; Gonzales et al. 2010, 2012; Schaerer & de Barros 2010) and that low luminosity galaxies are dominant during the epoch of reionization. However this would lead to more efficient generation of LW and IR backgrounds what in turn would slow down formation of the low mass galaxies. Perhaps a more

promising way to alleviate this problem is to take into account the non thermal radiation of matter accreted onto black holes what changes the spectrum of UV background, decreases the LW background and promotes the ionization of the Universe. Perhaps this effect can be observed as small distortion of the background light caused by emission in the He lines such as $\lambda = 304\text{\AA}$ and $\lambda = 584\text{\AA}$ shifted to the redshift of reionization $z_{ri} \sim 10 - 15$. More detailed discussion of these problems can be found in Meiksin (2009); Trenti et al. (2009, 2010); Shull et al. (2011); Giallongo et al. (2012); Barone–Nugent (2013); Ceverino et al. 2013).

Numerical simulations provide a powerful method of investigation of the epoch of reionization (e.g., Wise & Abel, 2007, 2008; Greif et al. 2008) and makes it possible to study the evolution of first galaxies in more details. In particular, they allow to investigate the early anisotropic stages of halo formation, to trace the process of the halo virialization, formation of its internal structure and early stages of protostar formation. Such analysis can be performed in a wide range of halo masses and redshifts what allows to improve the description of properties of relaxed halos of galactic scale and to link them with the power spectrum of initial perturbations.

However, possibilities of such simulations are strongly limited. These simulations are performed within a small box with the comoving size $L \sim 0.7 - 1.5$ Mpc what corresponds to the box mass $M_{box} \sim 10^{10} M_{\odot}$. So small box size artificially suppresses the large scale perturbations and the formation of more massive objects, what strongly distorts the simulated mass function and increases the expected number of low mass objects. Small box distorts also the influence of neighboring objects, the radiation transfer and the feedback of UV, LW and IR backgrounds. The star formation, their radiation, explosion and metal production cannot be simulated and are introduced by hand as independent factors. This list of limitations can be continued.

It is therefore interesting to consider a more rough but simple model of formation and evolution of early galaxies. In this paper we propose to use for such analysis the semi analytic approach based on the approximate analytical description of the basic DM structure of collapsed halos and numerical estimates of the thermal evolution of the baryonic component. During the last fifty years similar models have been considered and applied to study various aspects of non-linear matter evolution (see, e.g., Peebles 1967; Zel'dovich & Novikov 1983; Fillmore and Goldreich 1984; Gurevich & Zybin 1995; Bryan & Norman 1998; Lithwick & Dalal 2011). In this regard it is important to note that the DM halos are formed before stars appear (see, e.g., Kaviraj et al. 2013).

Formation of DM halos is a complex process with strongly anisotropic matter collapse during both earlier and final periods. Moreover sometimes this process is interrupted by the violent merging of neighboring halos. This implies that the simple spherical model of halos formation can not adequately to describe the present observational data. However properties of the steady state virialized DM objects are mainly determined by the integral characteristics of protoobjects and are only weakly sensitive to details of their evolution. This is clearly seen in numerous simulations which show that the Navarro – Frenk – White (NFW) density profile is very stable and is formed in majority of simulated DM halos.

The same simulations show also that properties of the cores of virialized DM halos are established during the early period of halos formation and later on the slow pseudo-evolution of halos dominates (see, e.g., Diemer et al. 2013). This means that properties of halo cores only weakly depend on the halo periphery and are determined mainly by their mass and the redshift of formation (Klypin et al. 2011). Using these results we formulate a rough two parametric description of all the basic properties of DM halos. These parameters are the virial mass of halos and the redshift of their formation.

First of all this approach allows us to reveal the close correlation between the redshift of formation and virial masses of halos with the initial power spectrum of density perturbations. It also allows to reconsider some of the widely discussed scaling relations between observed characteristics of galaxies (see, e.g., Spano et al., 2008; Donato et al. 2009; Gentile et al. 2009; Hyde & Bernardi, 2009; Salucci et al. 2011; Mosleh et al. 2011; Besanson 2013). Usually they are related to properties of luminous matter, such as fundamental plane, luminosity - velocity dispersion, or mass – size relations. Non the less they actually characterize the mass and entropy profile of halos and its formation in the course of violent relaxation of the compressed DM component.

Of course this approach is applied for the DM dominated halos only as the dissipative evolution of the baryonic component distorts properties of the cores of DM halos. In spite of this we can use this model in three ways:

- (i) The density and temperature profiles of the DM component can be considered as the initial conditions for numerical analysis of the process of cooling and compression of the baryonic clouds within the stable DM halos. In particular, with this approach it was possible to estimate the evolution of the Jeans mass of cold baryons down to the masses of Pop. III stars.
- (ii) We can use the redshift of the DM halos formation as a parameter that characterizes the 'frozen' properties of the central region of DM halos. This redshift correlates with the virial mass of halos and so with the initial power spectrum. Thus this approach allows us to reveal the impact of initial conditions on the observed characteristics of the DM dominated objects.
- (iii) This approach allows us to clarify also some of the widely discussed scaling relations that are applied to the DM dominated objects.

However potential of such approach should not be overestimated. Thus clusters of galaxies presented in Pratt et al. (2009) illustrate large scatter of matter distribution in the observed DM halos.

This paper is organized as follows. In Sec. 2 the basic relations and assumptions of our approach are formulated and the expected properties of the DM halos are presented. Properties and evolution of the baryonic component are described in Sec. 3. Mass dependence of the redshift of formation and the scaling relations for observed object are considered in Sec. 4. Discussion and conclusions can be found in Sec. 5.

1.1 Cosmological parameters

In this paper we consider the spatially flat Λ CDM model of the Universe with the Hubble parameter, $H(z)$, the critical

density ρ_{cr} , the density of non relativistic matter, $\langle\rho_m(z)\rangle$, and the mean density and mean number density of baryons, $\langle\rho_b(z)\rangle$ & $\langle n_b(z)\rangle$, given by:

$$H^2(z) = H_0^2[\Omega_m(1+z)^3 + \Omega_\Lambda], \quad H_0 = 100h \text{ km/s/Mpc},$$

$$\langle\rho_m(z)\rangle = 2.5 \cdot 10^{-27} z_{10}^3 \Theta_m \frac{g}{\text{cm}^3} = 3.4 \cdot 10^4 z_{10}^3 \Theta_m \frac{M_\odot}{\text{kpc}^3},$$

$$\langle\rho_b(z)\rangle = \frac{3H_0^2}{8\pi G} \Omega_b(1+z)^3 \approx 4 \cdot 10^{-28} z_{10}^3 \Theta_b \frac{g}{\text{cm}^3}, \quad (1)$$

$$\rho_{cr} = \frac{3H^2}{8\pi G}, \quad z_{10} = \frac{1+z}{10}, \quad \Theta_m = \frac{\Omega_m h^2}{0.12}, \quad \Theta_b = \frac{\Omega_b h^2}{0.02}.$$

Here $\Omega_m = 0.24$ & $\Omega_\Lambda = 0.76$ are dimensionless density of non relativistic matter and dark energy, $\Omega_b \approx 0.04$ and $h = 0.7$ are the dimensionless mean density of baryons, and the Hubble constant measured at the present epoch. Cosmological parameters presented in recent publication of the PLANCK collaboration (Ade et al. 2013) slightly differ from those used above (1).

For the Λ CDM cosmological model the evolution of perturbations can be described with sufficient precision by the expression

$$\delta\rho/\rho \propto B(z), \quad B(z)^{-3} \approx \frac{1 - \Omega_m + 2.2\Omega_m(1+z)^3}{1 + 1.2\Omega_m} \quad (2)$$

(Demianski, Doroshkevich, 1999, 2004; Demianski et al. 2011) and for $\Omega_m \approx 0.25$ we get

$$B^{-1}(z) \approx \frac{1+z}{1.35} [1 + 1.44/(1+z)^3]^{1/3}, \quad (3)$$

For $z = 0$ we have $B = 1$ and for $z \geq 1$ $B(z)$ is reproducing the exact value with accuracy better than 90%.

For $z \gg 1$ these relations simplify. Thus, for the Hubble constant and the function $B(z)$ we get

$$H^{-1}(z) \approx \frac{2.7 \cdot 10^{16}}{\sqrt{\Theta_m}} s \left[\frac{10}{1+z} \right]^{3/2}, \quad B(z) \approx \frac{1.35}{1+z}, \quad (4)$$

2 PHYSICAL MODEL OF HALOS FORMATION

As is commonly accepted in the course of complex nonlinear condensation the DM forms stable virialized halos with more or less standard density profile. Numerical simulations show that after short period of rapid evolution the structure of the virialized DM halos is quite well described by the spherical model with the Navarro – Frenk – White (NFW) density profile (Navarro et al. 1995, 1996, 1997; Ludlow et al., 2013). The basic parameters of the model – the virial mass, M_{vir} , central density, ρ_c , core scale r_s , and concentration, c , – were fitted in a wide range of redshifts and halo masses in many papers (see, e.g. Klypin et al. 2011).

After the completion of active phase of halo formation its parameters only weakly depend on the redshift and at large radius a steeper asymptotic density profile is formed,

$$\rho(r) \propto r^{-4},$$

(see, e.g., discussion in Visbal, Loeb, & Hernquist, 2012). But as before the central regions of halos are described by the NFW profile. For example such virialized objects are observed as isolated galaxies with the rotation curve $v_c \propto r^{-1/2}$

and/or as high density galaxies within clusters of galaxies, filaments or other elements of the Large Scale Structure of the Universe.

These results can be successfully used to roughly estimate the mean density and temperature of early galaxies what in turn allows us to concentrate main attention on the thermal evolution of the compressed gas. In this way we can consider the evolution of baryonic component and the formation of the first stars for a wide range of redshifts and virial masses of DM halos. Evidently similar approach can be applied also for investigations of more complex evolution of halos with the metal enriched baryonic component. This approach allows us also to estimate the redshift when the observed DM dominated objects such as the dSph galaxies and clusters of galaxies were formed.

It is important that the standard description of both the observed and simulated DM halos links the virial mass and radius of halos by the condition

$$M_{vir} = 4\pi/3 R_{vir}^3 \Delta_v \langle\rho_{cr}(z_{cr})\rangle, \quad (5)$$

where z_{cr} is the redshift of relaxation of DM halo, $\Delta_v = 18\pi^2 \approx 200$ and $\langle\rho_{cr}(z_{cr})\rangle$ is the critical density of the Universe at this redshift. This relation can be applied for halos embedded in a homogeneous medium – early galaxies and clusters of galaxies – and the value of Δ_v was derived from the simple model of spherical collapse that ignores the influence of complex anisotropic halos environment (see, e.g., Bryan & Norman 1998; Vikhlinin et al. 2009; Lloyd–Davies et al. 2011).

Of course, this approach has only limited predictive power. Thus, it ignores the complex anisotropic matter compression within filaments and walls before formation of compact halos, it ignores the effects produced by mergers and so on. These restrictions do not allow us to consider the process of generation of the angular momentum of the compressed matter and to link the properties of DM halos and the rate of star formation with the primordial characteristics of collapsed matter such as the anisotropic shape of density peaks and their environment, the internal velocity dispersion and so on. Non the less with this approach further progress in the description and understanding of the complex processes of formation of DM halos and early galaxies can be achieved.

2.1 Internal structure of DM halos

Further on we consider the virialized spherical DM halos characterized by the virial mass $M_{vir} = 10^9 M_\odot$ at the (conventional) redshift of formation $z = z_{cr}$. For any model the universal mass, M , and density, ρ , profiles of virialized DM halo can be taken as follows:

$$M(x) = M_c f_m(x), \quad \rho(x) = \rho_c f_\rho(x), \quad M_c = 4\pi\rho_c r_s^3. \quad (6)$$

Here $x = r/r_s$ and $r_s(M_{vir}, z_{cr})$, & $\rho_c(M_{vir}, z_{cr})$ are the typical size and density of the halos cores. For the popular NFW model the density and mass profiles are

$$f_\rho = x^{-1}(1+x)^{-2}, \quad f_m = \ln(1+x) - \frac{x}{1+x}, \quad (7)$$

and $f_m(5) \simeq 1$. For another popular model (Burkert, 1995) the density profile is

$$f_\rho = (1+x)^{-1}(1+x^2)^{-1},$$

$$f_m = \ln[(1+x)\sqrt{1+x^2}] - tg^{-1}(x), \quad f_m(5) \simeq 1.8. \quad (8)$$

These models can be used for $x \leq 5 - 6$. From these expressions it follows that at $x \geq 1$ differences between these models are quite moderate and our results obtained below for the NFW model can be applied with small corrections also for the Burkert model. More detailed discussion of these models can be found in Penarrubia et al. (2010).

Both the DM and baryonic components are treated as the ideal gas with the pressure, P , temperature, T , and the entropy function, S , linked by the usual expressions for the non relativistic particles:

$$P(x) = n(x)T(x) = S(x)n^{5/3}(x), \quad (9)$$

$$P(x) = P_c f_p(x), \quad T(x) = T_c f_T(x), \quad S(x) = S_c f_s(x),$$

where the typical temperature, $T_c(M_9, z_{cr})$, entropy, $S_c(M_9, z_{cr})$, pressure, $P_c(M_9, z_{cr})$ and the number density of the DM component, $n_{DM}(M_9, z_{cr})f_p(x)$, or baryons, $n_b(M_9, z_{cr})f_p(x)$, also depend upon the virial halo mass M_9 and its redshift of formation, z_{cr} .

Random variations of the profile and amplitude of the initial velocity, the initial shape of collapsed clouds, properties of outer regions of halos and so on lead to random variations of halos density, shape, profile and other parameters relative to the accepted mean characteristics. The analysis of available simulations shows that the probability distribution functions (PDFs) of these variations are often close to the exponential ones and therefore their random scatter is close to the mean values (see, e.g., Press & Rybicki, 1993; Demianski et al. 2011). These random variations can change the real parameters by a factor of 2 - 3.

2.2 Simple model of early galaxies

In this paper we consider a simple physical model of formation of galaxies based on the following assumptions:

(i) We assume that at redshift $z = z_{cr}$ the evolution of DM perturbations results in the formation of spherical virialized DM halos with mass $M_{vir} = M_9 \cdot 10^9 M_\odot$ and the density profile (7).

(ii) We do not discuss the dynamics of DM halos formation and evolution which are accompanied by the progressive matter accretion, the growth of the halos masses and corresponding variations of other halos parameters. The real process of halos formation is extended in time what causes some ambiguity in their parameters such as the halos masses and the redshift of their formation (see, e.g. discussion in Die-mand, Kuhlen & Madau 2007; Kravtsov & Borgani 2012). In the proposed model the redshift of halo formation, z_{cr} , is identified with the redshift of collapse of the homogeneous spherical cloud with the virial mass M_{vir} ,

$$1 + z_{cr} \approx 0.63(1 + z_{tr}), \quad (10)$$

where z_{tr} is the redshift corresponding to the turn around moment of the cloud evolution (see discussion in Umemura, Loeb & Turner 1993).

(iii) We assume that in the course of DM halo formation the main fraction of the baryonic component is heated by the accompanied shock waves up to the temperature and pressure comparable with the virialized values of the DM

component. These processes provide the formation of equilibrium distribution for the baryonic component.

(iv) We assume that some part of the compressed baryons is disrupted into a system of subclouds which are rapidly cooled and transformed into high density starlike subclouds. Thus, the virialized halo configuration is composed of the DM particles, the adiabatically compressed hot low density baryonic gas, and cold high density baryonic subclouds.

(v) Following Hutchings (2002) we assume that the cooling of the high density baryonic subclouds with both atomic (H & He) and molecular (H_2) coolants proceeds under the condition that $P \sim const$. Such cooling of the low mass subclouds corresponds to the isobaric mode of the thermal instability.

(vi) We assume that the subclouds with masses larger than the Jeans mass $M_J(n, T)$ rapidly form first stars with masses $100 - 1000 M_\odot$ what transforms the DM halos into the early galaxies.

The evolution of the cooled low mass subclouds can be very complex. It can be approximated by the isobaric mode of the thermal instability and therefore it does not preserve the compact shape of the cooled subclouds. As was discussed in Doroshkevich and Zel'dovich (1981) the motion of such subclouds within the hot gas leads to their deformation and less massive subclouds could be even dissipated. The complex aspherical shape of such subclouds makes their survival problematic and requires very detailed investigation to predict their evolution. It is very difficult to estimate also the efficiency of transformation of protostars into stars. These problems are beyond the scope of this paper.

In central regions of halos the gas pressure is supported by adiabatic inflow of high entropy gas from outer regions of halos what leads to progressive concentration of baryonic component within central regions of halos and to formation of massive baryonic cores (see, e.g. Wise & Abel 2008; Pratt et al. 2009). The structure and evolution of such halos resemble the internal structure of the observed and simulated galaxies and cluster of galaxies (see, e.g., Pratt et al. 2009, 2010; Arnaud et al. 2010; Kravtsov & Borgani 2012).

2.3 Mean characteristics of the DM halos

In this section we consider evolution of the central regions of virialized DM halos using the NFW approximations presented in Klypin et al. (2011), Prada et al. (2011), Angulo et al. (2012). For such halos of galactic scale and at $z \gg 1$ the matter concentration $c(M_9, z_{cr})$ is described by the expression

$$c = R_{vir}/r_s \approx 4M_9^{1/6} z_f^{7/3} \delta_r^{1/3} \epsilon, \quad z_f = (1 + z_{cr})/10, \quad (11)$$

$$\epsilon(M, z_{cr}) \approx 1 + 0.31M_9^{-1/4} z_f^{-4}, \quad M_9 = M_{vir}/10^9 M_\odot.$$

Here R_{vir} is the virial radius of halo and the factor $\delta_r^{1/3} \sim 0.6 - 1.4$ characterizes the random scatter of the matter concentration caused by the random variations of characteristics of the outer regions of halos. It is important that here we consider expected properties of early galaxies for which $M_9 z_f^{16} \geq 1$, $\epsilon \sim 1$. The usually discussed model of clusters of galaxies with $\epsilon \gg 1$ is considered below in Section 4.

Using the standard relations (5, 6)

$$M_{vir} = 4\pi\rho_c r_s^3 f_m(c) = 4\pi/3 R_{vir}^3 \langle\rho_{vir}\rangle, \quad \langle\rho_{vir}\rangle = \Delta_v \langle\rho_m\rangle,$$

we find the virial and core sizes of the halo,

$$R_{vir} \approx 3.34 \frac{M_9^{1/3}}{z_f} kpc, \quad r_s = \frac{R_{vir}}{c} = \frac{0.8 M_9^{1/6}}{z_f^{10/3} \delta_r^{1/3} \epsilon} kpc. \quad (12)$$

For the central density of the DM matter, ρ_c , and its number density, n_{DM} , we get

$$\rho_c(M, z) \approx \frac{\langle \rho_m \rangle \Delta_v c^3}{3 f_m(c)} \approx 1.3 \cdot 10^8 z_f^{10} M_9^{1/2} \Theta_\rho \frac{M_\odot}{kpc^3}, \quad (13)$$

$$n_{DM} = \frac{\rho_c}{m_{DM}} = 6 z_f^{10} M_9^{1/2} \Theta_\rho \frac{m_b}{m_{DM}} cm^{-3}, \quad \Theta_\rho = \frac{\delta_r \epsilon^3}{f_m(c)}.$$

Here $\delta_r \sim 0.1 - 3$ characterizes the discussed above random variations of the halo parameters relative to the mean characteristics presented by (13).

As was noted in the introduction the important characteristic of DM halos is the central surface density of the DM component, μ_{cs} , (Donato et al. 2009; Salucci et al. 2011)

$$\mu_{cs} = r_s \rho_c \approx 10^2 (M_9 z_f^{10})^{2/3} \Theta_\mu M_\odot / pc^2, \quad (14)$$

with $\Theta_\mu = \delta_r^{2/3} \epsilon^2 / f_m(c)$. The similar virial surface density,

$$\mu_{vir} = R_{vir} (\rho_{vir}) = 22.7 M_9^{1/3} z_f^2 \Theta_m M_\odot / pc^2, \quad (15)$$

is close in some respects with such phenomenological concepts as the Fundamental Plane or mass – size relation which also are discussed in many publications (see, e.g., Hyde & Bernardi, 2009; Mosleh et al. 2011; Besanson 2013).

The velocity dispersion, $\sigma_v^2(r)$, and the temperature, $T_{DM}(r)$, within the relaxed DM halo with the NFW density profile are closely linked to the circular velocity of DM halos, $v_c^2(r)$,

$$v_c^2(r) = \frac{GM(r)}{r} = \sigma_0^2 \frac{f_m(x)}{x}, \quad \sigma_v^2(x) \approx \frac{v_c^2(x)}{2\sqrt{x}} = \sigma_0^2 \frac{f_m(x)}{2x^{3/2}},$$

$$\sigma_0^2 \approx 4.5 \cdot 10^3 M_9^{5/6} z_f^{10/3} \Theta_T km^2/s^2, \quad \Theta_T = \epsilon \delta_r^{1/3} / f_m(c),$$

where again $x = r/r_s$. Thus for the temperature of DM component with Maxwellian velocity distribution we have

$$T_{DM} = m_{DM} \sigma_v^2 / 3 = T_c f_T(x), \quad f_T(x) = f_m(x) / x^{3/2},$$

$$T_c \approx m_{DM} \sigma_0^2 / 6 \approx 1.1 \cdot 10^5 M_9^{5/6} z_f^{10/3} m_{DM} / m_b \Theta_T K. \quad (16)$$

For the pressure of the DM component we get

$$P_{DM} = n_{DM} T_{DM} = P_c f_p(x), \quad f_p(x) = f_T(x) f_\rho(x),$$

$$P_c \approx 0.4 (M_9 z_f^{10})^{4/3} \Theta_p keV/cm^3, \quad \Theta_p = \Theta_\rho \Theta_T. \quad (17)$$

Here m_{DM} and m_b are the masses of DM particles and baryons. For the NFW model the pressure at the center of halo is divergent, $f_p(x) \propto x^{-1/2}$ what is another manifestation of the known core – cusp problem. This artificial divergence does not prevent the use of estimates (16) and (17) in our further discussions.

As is seen from this analysis the NFW halos are a two parametric sample and all the mean halos properties are determined by the redshift of halos formation, $z_f = (1 + z_{cr})/10$, and their virial masses M_{vir} . This is the direct result of the fixed density profile (7) and the expression for the matter concentration (11).

For the Burkert model we have no quantitative fits for the halo concentration. However comparing (7) and (8) we

can expect that the variations of the central density profile only weakly influence the characteristics of the matter distribution in halos at $x \geq 1$ and thus to obtain typical characteristics for any halos we can use the relations (11)–(17). In this case for Burkert profile the function $f_p(x)$ at $x \leq 1$ is similar to the isothermal one,

$$f_p(x) = f_\rho(x) f_m(x) / x^{3/2} \simeq p_0 - p_1 x^{3/2} + \dots, \quad (18)$$

what eliminates the divergence of pressure at $x = 0$ in (17). At $x \geq 1$ the function $f_p(x)$ is close to that obtained in (17) for the NFW model.

This means that at $x \geq 1$ differences between results obtained for various density profiles are in the range of random scatter. Results obtained for the generalized NFW model (Nagai, Kravtsov, & Vikhlinin 2007) confirm that numerical results are only weakly sensitive to moderate variations of the pressure and density profiles.

3 EVOLUTION OF THE BARYONIC COMPONENT

In the course of formation of galaxies the evolution of the baryonic component is driven by the evolution of the dominant DM component. In particular, the pressures of compressed DM and baryonic components are the same. However other properties of these components differ in many respects. Thus some fraction of baryons is compressed adiabatically, while other fraction is compressed by shock waves. Both fractions are compressed up to the pressure $P_{DM}(x)$ but their density, temperature and further evolution are different. Thus the shock compression is unstable and is accompanied by gas disruption into numerous subclouds. The low mass fraction of such subclouds can be transformed into Population III stars. Hot low density baryons form gaseous component of halos.

3.1 Adiabatically compressed baryonic component

In virialized halos the pressures of baryonic and DM components are equal to each other, $P_b(x) = P_{DM}(x)$. Therefore for a given $P_b(x)$ properties of the adiabatically compressed gas depend upon the relic entropy of baryonic component, S_{rel} . This entropy can be determined from the condition that at $z \sim 100 - 300$ the temperatures of baryons and relic radiation are close to each other. For example at $z = 100$ we have $T_b(100) \approx 2.7 \cdot 10^2 \approx 0.023 eV$, $\langle n_b(100) \rangle \approx 0.24 cm^{-3}$ and the relic entropy of baryons is

$$S_{rel} \approx S_0 = T_b(z) \langle n_b(z) \rangle^{-2/3} \approx 0.06 eV cm^2 \frac{100}{1+z}, \quad (19)$$

At the same time the relic (frozen) concentration of electrons and protons at $z \leq 100$ is small, $f_e = f_p \approx 10^{-4}$ what decelerates the formation of H_2 molecules and prevents cooling of the baryonic component below the temperature $T_b(x) \leq 10^4 K$. This means that for this component

$$P_b(x) = P_{DM}(x), \quad T_b = T_{bc} f_P^{2/5}(x), \quad n_b = n_{bc} f_P^{3/5}(x),$$

where the function $f_P(x)$ is determined by (17, 18) and

$$T_{bc} = S_{rel} (P_c / S_{rel})^{2/5} \approx 2 (M_9 z_f^{10})^{8/15} \Theta_{bc} eV, \quad (20)$$

$$n_{bc} = (P_c / S_{rel})^{3/5} \approx 2 \cdot 10^2 (M_9 z_f^{10})^{4/5} \Theta_p / \Theta_{bc} cm^{-3}.$$

$$\Theta_{bc} = \epsilon^{8/5} \delta_r^{8/15} f_m^{-4/5} (c)(S_{rel}/S_0)^{3/5}.$$

If the mass and the redshift of formation of the clouds of gas are limited by the condition

$$T_b(x) \leq 10^4 K,$$

or by the corresponding restriction for the pressure

$$P \leq 50 eV/cm^3 (T_b/10^4 K)^{5/2} (S_0/S_{rel})^{3/2}, \quad (21)$$

$$M_9 z_f^{10} \leq 0.2 \Theta_p^{-3/4} (T_b/10^4 K)^2 (S_0/S_{rel}),$$

then the cloud evolves in the adiabatic regime and the Jeans mass of the collapsed clouds M_J remains large

$$S_{bar} \approx S_{rel}, \quad M_J \approx 2.4 \cdot 10^5 M_\odot (1 cm^{-3}/n_{bc})^{1/2}. \quad (22)$$

In this case formation of the real stars is strongly suppressed.

However, if the condition (21) is violated and the collapsed gas is heated up to temperature $T_b(x) \geq 10^4 K$ then the concentrations of both electrons and H_2 molecules are rapidly increasing, gas is cooled and forms the high density low mass baryonic subclouds. The same process rapidly occurs also when the matter ionization is caused by external sources of the UV radiation.

3.2 Formation of high density baryonic subclouds

Some fraction of the baryonic component is compressed and heated in the shock waves generated in the course of the matter infall into the DM potential well. For this fraction the pressure, velocities and temperature of both baryonic and DM components are quite similar to each other and are given by expressions (16, 17):

$$P_b(x) = P_{DM}(x), \quad T_b(x) \approx T_{DM}(x) m_b/m_{DM}. \quad (23)$$

In this case the density and entropy of the shock compressed gas are

$$n_b(x) \approx P_b(x)/T_b(x) \approx 44 z_f^{10} M_9^{1/2} \Theta_\rho f_\rho(x) cm^{-3}, \quad (24)$$

$$S_{bar}(x) = P_b/n_b^{5/3} \geq S_{rel},$$

where the function $f_\rho(x)$ and the parameter Θ_ρ were defined above.

Instability of the shock compression and heating of baryons and their subsequent cooling lead to their fragmentation and formation of subclouds with high n_b and small T_b . If the formation of DM halo occurs with the cosmological characteristic time,

$$t_{cosm} = H^{-1}(z) \approx 2.7 \cdot 10^{16} z_f^{-3/2} s,$$

then the characteristic hydrodynamical time for the shock compressed baryonic component at $z_f \geq 1$ is much smaller,

$$\tau_{hyd} = \frac{1}{\sqrt{4\pi G \rho_b}} \sim \frac{1.4 \cdot 10^{14} s}{M_9^{1/4} z_f^5 \Theta_\rho^{1/2}} f_\rho^{-1/2}(x) \ll H(z)^{-1}, \quad (25)$$

and cooling of the highly ionized compressed gas occurs even more rapidly. For instance for the free – free cooling the characteristic time, τ_{ff} , is

$$\tau_{ff} \simeq \frac{5 \cdot 10^{12} s}{z_f^8 M_9^{1/2}} \frac{\Theta_T^{1/2}}{\Theta_\rho} \frac{f_T^{1/2}(x)}{f_\rho(x)} \ll \tau_{hyd}. \quad (26)$$

The impact of other atomic processes (recombination and excitation of H and He etc.) significantly decreases even this

characteristic time. The characteristic time for the hydrogen recombination is also quite small,

$$\tau_{rec} \approx 3.1 \cdot 10^{11} s z_f^{-8.4} M_9^{0.06} \Theta_\rho f_\rho(x) / \sqrt{\Theta_T f_T(x)} \ll \tau_{hyd},$$

what ensures almost equilibrium ionization of baryons throughout the period of thermal evolution for $T_b \geq 10^4 K$.

However for temperature $T_b \leq 10^4 K$ the cooling process determined by the molecular hydrogen is slower and the characteristic time of gas cooling becomes comparable with τ_{hyd} (25). This means that the gas pressure within cold subclouds is retained near $P_b(x)$ (23) and the cooling is accompanied by a corresponding growth of baryonic density.

Owing to the thermal instability such evolution strongly favors further fragmentation of the cooled gas. The gravitationally bounded cold high density subclouds with masses larger than the Jeans mass, $M \geq M_J$, could be transformed into stars. The formation of stars with the mass M_{st} is regulated by the drop of temperature, $T_4 = T_b/10^4 K$,

$$M_{st} \geq M_J \approx 2 \cdot 10^7 M_\odot \frac{T_4^{3/2}}{n_3^{1/2}} = \frac{2.5 \cdot 10^6 M_\odot T_4^2}{(M_9 z_f^{10})^{2/3}} \sqrt{\frac{5}{\Theta_\rho}}, \quad (27)$$

where $n_3 = n_b/1 cm^{-3}$ is the number density of cooling gas. Some part of the gas is concentrated near the center of the host DM halo (Wise & Abel 2008; Pratt et al. 2009 2010) forming the baryonic core.

3.3 Numerical estimates

The cooling process of the baryonic component can be followed numerically by solving the equations of thermal balance and evolution of nine components, namely, the electrons, e , protons, p , neutral and molecular hydrogen, H & H_2 , ions H^- & H_2^+ , and neutral and ionized helium, He , He^+ , He^{++} . The kinetic coefficients and the cooling rates used here are taken from Hutchings et al. (2002).

As is well known there are two different regimes of cooling of the compressed gas. Thus, very slow cooling takes place when temperature of the compressed gas (16, 23) does not exceed $\sim 10^4 K$. In this case the low electron concentration $y_e = n_e/n_b \sim 10^{-4}$ created at high redshifts $z \sim 100$ remains unchanged, the formation of molecules H_2 and gas cooling are slow and formation of starlike subclouds is strongly delayed. On the other hand when temperature of the compressed gas (16, 23) exceeds $10^4 K$ and the strong ionization of hydrogen takes place then the concentrations of both electrons and molecules H_2 strongly increase, the compressed gas rapidly cools down to temperature $T_b \simeq 100 K$ and forms starlike high density subclouds.

As is seen from (16, 23) temperature of the compressed baryons is a two parametric function. Thus for a given virial mass M_9 it rapidly decreases with z_{cr} and for some z_{cr} the threshold temperature $T_b \approx 10^4 K$ is reached. This means that at such z_{cr} the baryon cooling and the star formation process are strongly decelerated. In turn, for a given z_{cr} and halos of low virial masses the threshold temperature $T_b \approx 10^4 K$ cannot be reached. For such virial mass the star formation process becomes also suppressed. This means that star formation in low mass halos occurs mainly at higher redshifts while at $1+z_{cr} \sim 10$ stars cannot be formed within halos with $M_9 \leq 1$.

These statements are illustrated in Figs. 1 and 2 where

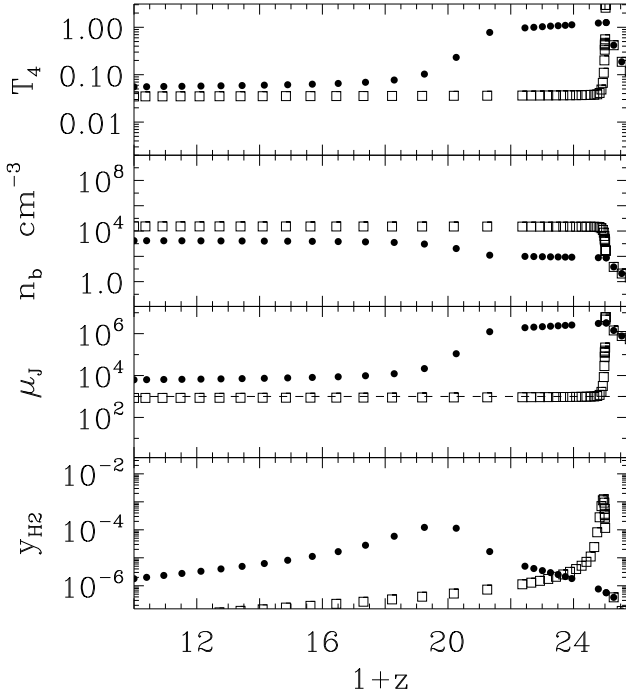


Figure 1. Redshift variations of the temperature, T_4 , baryonic number density, n_b , Jeans mass, $\mu_J = M_J/M_\odot$, and H_2 concentration, y_{H_2} , within halos formed at $z_{cr} = 25$, $z_f = 2.5$, with the virial masses $M_{vir} \approx 5 \cdot 10^5 M_\odot$ (points) and $M_{vir} \approx 9 \cdot 10^5 M_\odot$ (squares).

the thermal evolution of compressed gas is presented for two sets of halo masses and two redshifts of halo formation. As is seen in both Figures for less massive halos the rapid atomic cooling at $T_4 \geq 1$ is replaced by slower cooling with H_2 molecules at $T_4 \leq 1$. In contrast for more massive halos formed at the same redshift z_f the cooling rate with H_2 molecules remains quite rapid.

For two halos with virial mass $M_{vir} = 5 \cdot 10^5 M_\odot$ and $M_{vir} = 9 \cdot 10^5 M_\odot$ formed at $z_{cr} = 25$ the evolution of high density gaseous subclouds is presented in Fig. 1. The formation of gravitationally bounded subclouds is restricted by the Jeans mass, $\mu_J(z)$, which drops down to starlike value $M_J \simeq 10^3 M_\odot$ at redshifts $1+z \sim 16$ & 23 , correspondingly. Formation of less massive starlike subclouds is also hampered. This means that formation of halos with the virial masses $M \leq 10^6 M_\odot$ at redshifts $z_f \leq 2.5$ is not usually accompanied by a noticeable star formation.

Other example – evolution of two halos with masses $M_{vir} = 10^9 M_\odot$ and $M_{vir} = 0.3 \cdot 10^9 M_\odot$ formed at $z_f \sim 1$ is presented in Fig. 2. In this case the gravitationally bounded starlike subclouds with $M_{scl} \simeq M_J \approx 10^3 M_\odot$ can be formed at $1+z \leq 9.8$ & 7.5 , correspondingly. This means that at $z_f \leq 1$ even massive stars can be formed presumably within metal free halos with $M_{vir} \geq 10^9 M_\odot$.

3.4 Constrains on the star formation process

It can be expected that the first stars are formed at $z_{cr} \sim 20 - 30$ within rare DM halos with the low relic concentration of electrons $x_e \sim 10^{-4}$ and relic entropy of baryons (19). Both these values are determined at $z \sim 100 - 300$ after

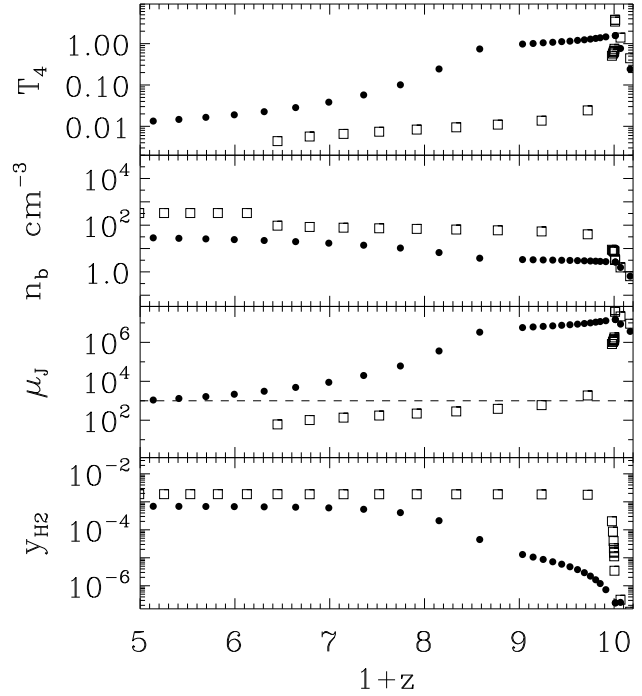


Figure 2. Redshift variations of the temperature, T_4 , baryonic number density, n_b , Jeans mass, $\mu_J = M_J/M_\odot$, and H_2 concentration, y_{H_2} , within halos formed at $1+z_{cr} = 10$, $z_f = 1.0$, with the virial masses $M_{vir} \approx 10^9 M_\odot$ (squares) and $M_{vir} \approx 0.4 \cdot 10^9 M_\odot$ (points).

the period of hydrogen recombination. As was shown above with such low concentration of electrons it is not possible to efficiently form H_2 molecules and to cool the gaseous component of low mass halos. However these processes are strongly accelerated when the temperature of the compressed baryonic component exceeds (conventional) level $T_{gas} = 10^4 K$. In this case thermal ionization of hydrogen takes place what rapidly increases the concentrations of both electrons and H_2 molecules, and accelerates cooling of the gaseous component and formation of starlike clouds.

This means that the condition (21) which restricts this temperature can be used as an approximate demarcation line on the plane M_{vir}, z_{cr} between regions of rapid and slow star formation. The more convenient presentation of this line is

$$M_{vir} \simeq 10^6 M_\odot \left[\frac{17.1}{1+z_{cr}} \right]^{10} \left[\frac{T_{bc}}{10^4 K} \right]^2 \frac{S_0}{S_{rel}} \Theta_p^{-3/4}. \quad (28)$$

As is seen from (28) for each mass of halo there is the minimal redshift of the halo formation, z_{cr} , for which the baryonic component is rapidly cooled and can form starlike objects. The halos with the primordial chemical composition that were formed at redshifts less than some minimal redshift, $z_{cr} \leq z_{min}(M_{vir})$, practically cannot produce Pop. III stars and ionizing photons. For example, as is seen from Fig. 1 for the halo with $M_{vir} = 0.5 \cdot 10^6 M_\odot$ formed at $z_{cr} \leq 25$ temperature of the compressed gas decreases very slowly and the star formation is strongly delayed. Similar results are presented in Fig. 2 for halos with the relic composition and masses $M_{vir} \leq 0.4 \cdot 10^9 M_\odot$ formed at $z_{cr} \leq 10$.

However it is necessary to note the approximate character of the relation (28) and its complex links with the pro-

cess of star formation and the masses of formed stars. More detailed analysis shows that the restriction (28) is eroded owing to the radial variations of temperature, possible ionization by the UV background, random variations of the initial perturbations and so on. This means that stars can be efficiently formed also in DM halos that are found in some strip around the line (28).

These results lead to important conclusions regarding the sources of the UV photons that caused the reionization of the Universe at redshifts $z \sim 10-11$ (Komatsu et al. 2011; Larson et al. 2011). As is seen from Eq. (28) at redshifts $z \simeq 10$ the halos with virial masses $M_0 \geq 1-10$ provide most of Population III stars with $M_{str} \sim 10^2-10^3 M_\odot$ while the contribution of less massive halos can be moderate. The contribution of low mass galaxies to the UV background is also suppressed by the feedback of supernova explosions (see, e.g., Wyithe et al. 2013; Salvadori et al. 2013; Ceverino et al. 2013).

3.5 Impact of the Lyman - Werner radiation

The constrain (28) is strongly enhanced when the disruption of H_2 molecules by the Lyman-Werner (LW) or H^- ions by the infrared (IR) photons becomes noticeable (see, e.g. discussion in Loeb & Barkana, 2001; Muñoz et al., 2009; Wolkott-Green & Haiman, 2012 and references therein). These photons are produced by thermal sources of radiation (such as stars) together with $Ly-c$ and more energetic photons. As is well known, for the strong reionization at $z \sim 10$ it is necessary to produce at least one $Ly-c$ photon per baryon. The allowance for the complex spectral distribution of the generated UV photons, ionization of He and the heating and recombination of the IGM can increase this estimate by a factor of 2-3. This is the minimal value and in some papers (see, e.g. Dijkstra, Haiman, Loeb 2004; Madau 2007) production of extra (up to 10) UV photons per baryon is discussed. But at the same time the thermal sources produce comparable number of LW photons with the density $n_{LW} \sim n_b \sim 3 \cdot 10^{-7} z^3 cm^{-3}$. Such flux of LW photons practically brings to a halt formation of H_2 molecules and first star (see, e.g., Safranek-Shrader et al., 2012).

However, generation of the LW photons is strongly suppressed when the ionization of the hydrogen and helium is provided by non thermal sources of the UV radiation. Such non thermal radiation is inevitably generated by matter accreted onto black holes created by explosions of massive and supermassive stars. But in contrast with the thermal sources the non thermal sources do not produce immediately the LW photons and do not decelerate the process of formation of first stars. At high redshifts the heating of the intergalactic gas by the soft X-ray background is not efficient owing to the cooling of ionized baryons by the inverse Compton scattering, free - free emission, excitations of the neutral hydrogen and so on. In this case we can expect the moderate increase of the Jeans mass up to

$$M_J \approx 4 \cdot 10^7 T_4^{3/2} z_f^{3/2} M_\odot,$$

and corresponding increase of masses of forming galaxies. However in this case the more efficient generation of the IR and hard UV backgrounds can be expected what leads to partial ionization of HeI and HeII. Perhaps this inference can be confirmed by observations of tracks of He lines such

as $\lambda = 304A$ and $\lambda = 584A$ shifted by redshift $1 + z_{cr} \geq 10$ to the region of visible spectrum.

Random spatial distribution of the first galaxies and random variations of generated UV radiation implies that realistic representation and analysis of the reionization process is possible only with the representative numerical simulations that consider at the same time both the process of star formation and generation of the UV and LW backgrounds. It can be expected that these processes are separated in space what requires a representative simulated volume together with a high resolution.

4 SCALING RELATIONS FOR THE DM DOMINATED OBJECTS.

Simulations show that characteristics of the virialized DM halos are much more stable than the characteristics of baryonic component and after formation at $z = z_{cr}$ of virialized DM halos with $\langle \rho_{vir} \rangle \approx 200 \langle \rho(z_{cr}) \rangle$ slow matter accretion only moderately changes their characteristics (see, e.g., Diemer et al. 2013). Because of this, we can observe earlier formed high density galaxies with moderate masses even within later formed more massive but less dense clusters of galaxies, filaments and other structure elements. This means that using the model presented in Sec. 2 for description of the observed dSph galaxies and clusters of galaxies dominated by DM component we can find one-to-one correspondence between their observed parameters and the so called redshift of object formation, z_{cr} . Of course according to the Press - Schechter approach (Press, Schechter, 1974; Peebles 1974) these redshifts characterize the power spectrum of the density perturbation rather than the real period of the object formation.

Following this approach to describe the halos formation we use the function $B(z_{cr})$ (3) rather than the redshift z_{cr} . For large $z_{cr} \gg 1$ the function $B(z_{cr})$ is equivalent to the redshift and we can use redshift z_{cr} for discussion of properties of the dSph galaxies. However many observed clusters of galaxies are situated at redshifts $z \leq 1$ and in this case these differences become significant.

The simplest way to estimate the redshift of halo formation is to use Eq. (5) which can be rewritten as

$$(1 + z_{cr})^3 = 3M_{vir}/4\pi R_{vir}^3/\Delta_v \langle \rho_m(z=0) \rangle.$$

However this approach has to deal with unstable ragged periphery of halos and to reasonably estimate the virial radius it is necessary to use a complex model dependent procedure.

More stable but more complex way is to use the expression (11) (or its equivalent) for the matter concentration and/or parameters of the central core - r_s & ρ_c . However in this case it is not possible to achieve high precision because of the possible impact of baryonic component, complex shape of these relations and complex procedures of measurement of these parameters. Non the less this approach has the largest potential to analyze the available observations.

Today the parameters of the virialized DM halos are known for some population of dSph galaxies (Walker et al., 2009, 2012; Tollerud et al. 2012) and for many clusters of galaxies (see e.g. Piffaretti et al. 2011; Kravtsov, Borgani 2012; McDonald 2013; and references below). Here we present some results of such analysis.

Perhaps this approach can be applied also for virialized groups of galaxies and for galaxies with measured rotation curves at large distances. However measurement of the virial radius and the mean density for such objects is problematic and more indirect approaches must be used for such analysis.

4.1 Redshift of formation of the dSph galaxies

Samples of the dSph and And (companions of the Andromeda galaxy) galaxies include objects in a wide range of masses, $0.1 \leq M_6 = M_{gal}/10^6 M_\odot \leq 100$, what allows us to reveal more reliably the mass dependence of their redshift of formation. Some observed properties of 28 dwarf DM dominated galaxies are compiled in Walker et al. (2009) and for 13 And galaxies are presented in Table 4 in Tollerud et al. (2012). In this case we have to deal with parameters of the central regions at the projected half-light radius. Moreover, the presented data are recalculated from actual observations (Walker et al. 2009; Walker 2012) and, so, their reliability is limited and scatter is large. In spite of this it is interesting to compare characteristics of these galaxies and observations of clusters of galaxies with the theoretical expectations of Sec. 3.

First of all for the sample of 28 dSph galaxies we can roughly estimate the dimensionless size of the region under consideration. To do this we compare the observed masses, radii and velocity dispersions with expectations (16). For this sample we get

$$\langle \sqrt{r_{ob}/r_s} \rangle \approx \left\langle \frac{GM_{ob}}{2r_{ob}\sigma_v^2} \right\rangle \approx 1.3 \pm 0.02.$$

This means that the observed values of M_{ob} , σ_v , & r_{ob} are related to the model parameters as follows:

$$r_{ob} \sim 1.7r_s, \quad M_{ob} \sim 0.36M_{vir}, \quad \langle \rho_{ob} \rangle \sim 0.1\rho_c. \quad (29)$$

For both the NFW and Burkert models these corrections are quite similar to each other because they consider regions where $r_{ob} \geq r_s$.

In order to find the redshift of object formation, $z_f = (1 + z_{cr})/10$, we can use two approaches. Firstly we can use the estimates of the central density (13) which can be expressed with the help of (29) through the observed M_{ob} and $\langle \rho_{ob} \rangle$

$$z_{f\rho}^{10} \approx \frac{150}{\sqrt{M_6}} \langle \rho_{ob} \rangle \frac{pc^3}{M_\odot}, \quad (30)$$

where $M_6 = M_{ob}/10^6 M_\odot$ is the observed mass of DM galaxy. The great advantage of this method is a weak dependence of z_{fr} on ρ_{ob} what attenuates the impact of errors. For comparison we can use expression (12) for the typical size of the central regions,

$$z_{fr}^{10/3} \approx 0.5M_6^{1/6}/r_{kpc}, \quad (31)$$

where r_{kpc} is the observed radius, r_{ob} , in kpc. Both estimates are quite similar to each other and we have

$$z_f \simeq z_{f\rho} \approx 0.9z_{fr}.$$

The redshifts of formation of galaxies are spread between values $1 + z_{cr} = 8$ for *Sgr*^c and $1 + z_{cr} = 20$ for Segue 1. The fit of the mass dependence of $z_{cr}(M)$ is

$$z_f M_6^{0.1} \approx 1.7(1 \pm 0.12),$$

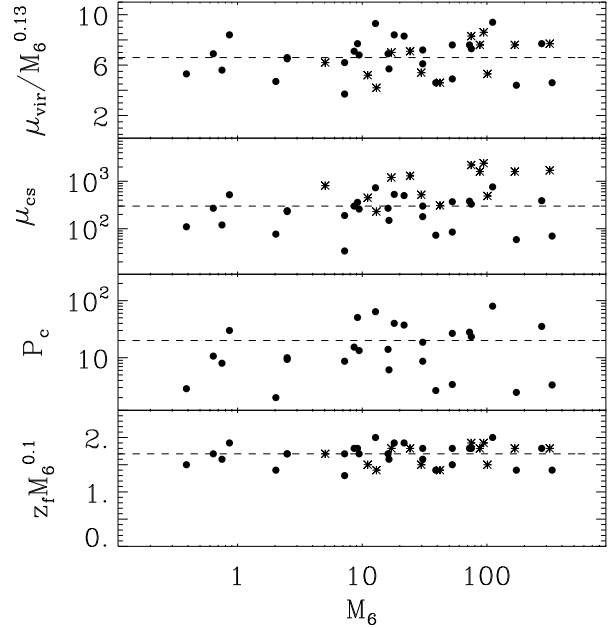


Figure 3. Functions $\mu_{vir}/M_6^{0.13}$, μ_{cs} , $P_c(M_6)$ and $z_f M_6^{0.1}$ are plotted for the observed samples of 28 dSph galaxies (points) and 13 And galaxies (stars). Fits (32), (34), (45) and (46) are plotted by dashed lines.

$$1 + z_{cr} \approx 17(1 \pm 0.12)M_6^{-0.1} \approx 3(1 \pm 0.12)M_{13}^{-0.1}, \quad (32)$$

These results are presented in Fig. 3.

For 13 And galaxies the masses and half-light radii are listed in Table 4 in Tollerud et al. (2012). For these objects we can use the expression (31) to estimate their redshift of formation. For this sample we get

$$z_f M_6^{0.1} \approx 1.6(1 \pm 0.11), \quad 1 + z_{cr} \approx 16(1 \pm 0.11)M_6^{-0.1}, \quad (33)$$

what is identical with (32). The maximal $1 + z_{cr} \approx 14$ is obtained for the galaxy And XVI.

These results are also presented in Fig. 3. However it is necessary to note that parameters of the galaxies And IX and And XV presented in both surveys are noticeably different.

Comparison of the relations (17) and (32) shows that the weak mass dependence can be expected also for the typical DM pressure, $P_c(M_{vir}, z_f)$. Analysis of the sample of dSph galaxies results in the following estimate

$$P_c(M_6) \approx 20(1 \pm 0.9)eV/cm^3. \quad (34)$$

This function is plotted in Fig. 3. It is very close to demarcation value (21) but is more sensitive to (random) scatter of the observed parameters than z_f .

Combining Eq. (32) with Eqs. (12) and (13) we can directly link parameters of the core and virial masses of halos

$$\rho_c \sqrt{M_{vir}} \approx const, \quad r_s / \sqrt{M_{vir}} \approx const. \quad (35)$$

However these links are not so strong and for these relations scatter can be as high as 50 – 100% what decreases their usefulness.

4.2 Redshift of formation of clusters of galaxies

Now there are more or less reliable observational data at least for ~ 300 clusters of galaxies (Ettori et al. 2004; Pointecouteau et al. 2005; Arnaud et al., 2005; Pratt et al., 2006; Zhang et al., 2006; Branchesi et al., 2007; Vikhlinin et al., 2009; Pratt et al. 2010; Suhada et al. 2012; Moughan et al. 2012; Babyk et al. 2012; Foéx et al. 2013; Bhattacharya et al. 2013). However, the main cluster characteristics are not directly observed and are obtained by a rather complex procedure (see, e.g., Bryan & Norman 1998; Vikhlinin et al. 2009; Lloyd-Davies et al. 2011; McDonald M., et al., 2013). In particular they relate the virial mass and radius of each cluster with the critical density of the Universe at the observed redshift, $\rho_c(z_{obs})$,

$$M_{vir} = 4\pi/3 R_{vir}^3 500 \rho_c(z_{obs}) = 250 R_{vir}^3 H^2(z_{obs})/G.$$

In fact this assumption identifies the redshift of cluster formation with the observed redshift. This assumption is questionable for majority of clusters as quite similar clusters are observed in a wide range of redshifts. It distorts all published cluster characteristics and often makes impossible to use the published characteristics of cores for further discussions. The matter concentration is measured with a reasonable precision only for 25 clusters of sample CLS-25 combined from samples CLS-10 (Pointecouteau et al. 2005), CLS-12 (Vikhlinin et al. 2006) and CLS-18 (Bhattacharya et al. 2013). The central regions of many clusters are influenced by cooling baryonic component (see, e.g., Pratt et al., 2009, 2010) but for these three samples the concentrations are determined with precision of $\sim 10 - 15\%$ what allows us to estimate the redshift of formation, z_{cr} , and both the central and the virial surface densities of clusters, $\mu_{cs} = r_s \rho_c$ and $\mu_{vir} = R_{vir}(\rho_{vir})$.

For this sample the redshift z_{cr} can be obtained from the relation (Dolag 2004):

$$1 + z_{cr} \approx \frac{11}{c(M_{vir, z_{cr}})M_{13}^{0.1}}, \quad M_{13} = M_{vir}/10^{13}M_{\odot}, \quad (36)$$

$$(1 + z_{obs}) = 1.09(1 \pm 0.05), \quad \langle c \rangle \approx 4.05 \pm 0.9,$$

$$(1 + z_{cr}) \approx 2.1(1 \pm 0.24). \quad (37)$$

The maximal values $1 + z_{cr} \approx 3.6$ and $1 + z_{cr} \approx 2.6$ are obtained for the cluster *MKW4* with $M_{13} \approx 7.7$ and for the cluster *A262* with $M_{13} \approx 8.3$ observed at $z_{obs} = 0.02$ and $z_{obs} = 0.016$ (Vikhlinin et al. 2006; Bhattacharya et al. 2013). For these clusters $z_{cr} \gg z_{obs}$ what confirms differences between the redshift of cluster formation and random observed redshift at least for clusters with $z_{obs} \ll 1$.

However as was noted above for redshifts $z_{cr} \leq 1$ the cluster formation is determined by the function $B(z)$ (3) rather than by the redshift z_{cr} . Thus for these samples we get

$$\langle B^{-1}(z_{cr}) \rangle \approx 1.63(1 \pm 0.2) = 2.3(1 \pm 0.2)M_{13}^{-0.1}. \quad (38)$$

This value is quite comparable with the estimates (32) which can be rewritten for dSph galaxies as follows

$$\langle B^{-1}(z_{cr}) \rangle \approx 2.22(1 \pm 0.12)M_{13}^{-0.1}. \quad (39)$$

However large scatter and uncertainties in both estimates (32) and (38) prevent more detailed comparison of these results.

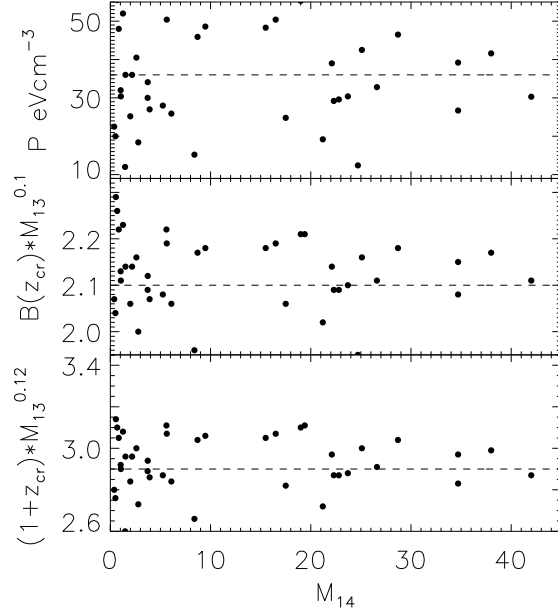


Figure 4. For 44 clusters from the sample CLS-83 the redshift formation, $(1 + z_{cr})M_{13}^{0.12}$ and $B(z_{cr})M_{13}^{0.1}$, and of the central pressure, P_c , are plotted vs. mass of clusters. Dashed lines show fits (42).

The more interesting sample CLS-83 (McDonald et al. 2013) contains parameters of central regions of 83 clusters with redshifts $z \geq 0.3$, namely, baryonic density and temperature, n_c & T_c . Using relations (23) and (24) we can estimate for these clusters the redshift of formation z_{cr} and mass M_{13}

$$M_{13} \approx 10^{-4} \left(\frac{44cm^{-3}}{n_c} \right)^{1/2} \left(\frac{T_c}{9.5eV} \right)^{3/2} f_m(c), \quad (40)$$

$$1 + z_{cr} \approx 10. \left(\frac{n_c}{44cm^{-3}} \right)^{1/8} \left(\frac{9.5eV}{T_c} \right)^{3/40} \epsilon^{-0.3}.$$

For 44 clusters of this sample with the central pressure $P_c = n_c T_c \leq 70 eV cm^{-3}$ we get

$$\langle P_c \rangle \approx 36(1 \pm 0.37) eV cm^{-3}, \quad (41)$$

$$\langle (1 + z_{cr}) \rangle \approx 2.9(1 \pm 0.05)M_{13}^{-0.12}, \quad 0.3 \leq z_{cr} \leq 1.5, \quad (42)$$

$$\langle B(z_{cr}) \rangle \approx 2.1(1 \pm 0.04)M_{13}^{-0.095}.$$

These results are plotted in Fig. 4.

It is important that in spite of the large difference in masses of these clusters ($M/M_{\odot} \geq 10^{13}$) and dSph galaxies with ($M/M_{\odot} \leq 10^9$) estimates (41) are very close to (34) while (42) are quite similar to (37)–(39). For other 39 clusters of this sample all characteristics are strongly distorted owing to cooling of gaseous component what significantly increases scatter of the final estimates.

4.3 Surface density of DM dominated objects

In set of publications (e.g., Spano et al., (2008); Donato et al. 2009; Gentile et al. 2009; Salucci et al., 2011) it is found that the central surface density, $\mu_{cs} = r_s \rho_c$, is almost the same across a wide range of galaxies of different types and luminosities. Thus for 36 spiral galaxies Spano et al. (2008) obtains

$$\langle \mu_{cs} \rangle \approx 150_{-70}^{+100} M_{\odot} pc^{-2}.$$

For the dSph galaxies Donato et al. (2009) estimates this surface density as

$$\langle \mu_{cs} \rangle \sim 140_{-30}^{+80} M_{\odot} pc^{-2},$$

while Salucci et al. (2011) infer that

$$\log(\rho_c) = -\alpha \log(r_s), \quad 0.9 \leq \alpha \leq 1.1.$$

Here we will check these inferences with the available data sets.

4.3.1 Surface density of the dSph galaxies

In Sec. 4.1 links between the core and virial parameters of the dSph galaxies and their redshift of formation were discussed. The weak mass dependence of the observed DM surface density of the same dSph objects is other demonstration of the same links. Indeed, as is seen from (14) the weak mass dependence of the function

$$\langle \mu_{cs} \rangle = r_s \rho_c \approx F_{srf}^{2/3} \Theta_{sc} M_{\odot} / pc^2, \quad \Theta_{sc} = \delta_r \epsilon^3 / f_m^{3/2}(c), \quad (43)$$

follows immediately from the weak mass dependence of the function

$$F_{srf} = M_6 z_f^{10} \simeq const., \quad (44)$$

which determines also the weak mass dependence of the redshift of formation z_{cr} discussed in Sec. 4.1. Here $c(M_9, z_{cr})$ is the concentration (11), and the virial dimensionless mass of objects $f_m(c)$ is given by (7) for the NFW density profiles.

Using the estimates (32) we get

$$\langle \mu_{cs} \rangle \approx 230 M_{\odot} / pc^2,$$

while the direct estimates with the full sample of 28 dSph galaxies give

$$\langle \mu_{cs} \rangle \approx 300(1 \pm 0.66 \pm 0.51) M_{\odot} / pc^2. \quad (45)$$

Here the first uncertainty is connected with the scatter of μ_{cs} over the sample, while the second one characterizes the precision of separate measurements. These results are presented in Fig. 3.

Large scatter of the surface density strongly decreases its significance and possible applications. Non the less for galactic scales the weak mass dependence of the surface density is confirmed by the weak mass dependence of the redshift of formation.

In accordance with (15) the virial surface density of dSph galaxies is weakly dependent on its virial mass and is described by the relation

$$\langle \mu_{vir} \rangle \approx 6.6 M_6^{0.13} (1 \pm 0.21) M_{\odot} / pc^2, \quad (46)$$

where as before $M_6 = M_{vir} / 10^6 M_{\odot}$ and $M_{vir} \approx M_{half} / 0.36$. This result is consistent with (32). The function $\mu_{vir} / M_6^{0.13}$ is plotted in Fig. 3.

4.3.2 DM surface density for clusters of galaxies

It is necessary to remind that if for galaxies we had $\epsilon(M, z_{cr}) \sim 1$ in relations (11) - (17) then for some clusters of galaxies $\epsilon \gg 1$ and we get for their DM surface density

$$\mu_{cs} \approx 204 \left[\frac{M_{13}}{(1+z_{cr})^4} \right]^{1/6} \Theta^* \frac{M_{\odot}}{pc^2}, \quad \Theta^* = \frac{\delta_r^{2/3} \epsilon^2}{f_m(c)}, \quad (47)$$

$$\epsilon = 1 + 3.7 \cdot 10^{-2} M_{13}^{1/4} (1+z_{cr})^4, \quad M_{13} = M_{vir} / 10^{13} M_{\odot}.$$

This means that relations (43, 44) which are valid for galaxies cannot be applied for massive clusters of galaxies.

Using the expression (47) with $\langle 1+z_{cr} \rangle$ estimated by (37) we get

$$\mu_{cs} \approx 124 M_{13}^{1/6} M_{\odot} / pc^2, \quad (48)$$

what is a rough estimate owing to the large scatter of z_{cr} . More accurate results can be obtained from expressions (5):

$$\mu_{cs} = \frac{M_{vir}}{4\pi r_s^2 f_m(c)} = \frac{100}{4\pi} \frac{M_{13}}{f_m(c)} \frac{c^2}{R_{Mpc}^2} \frac{M_{\odot}}{pc^2}, \quad (49)$$

where as before $c(M, z_{cr})$ is the halo concentration, $M_{13} = M_{vir} / 10^{13} M_{\odot}$, and R_{Mpc} is the virial radius of cluster in Mpc. With this relation we get for the sample CLS-25

$$\langle \mu_{cs} \rangle \approx 415(1 \pm 0.3) \frac{M_{\odot}}{pc^2} \approx 150(1 \pm 0.25) M_{13}^{0.3} \frac{M_{\odot}}{pc^2}. \quad (50)$$

This estimate differs from that obtained for galaxies (45) because it depends on mass. The fact that (48) and (50) are different shows that these results depend on the averaging procedure.

The virial surface density of clusters is closely linked with their central surface density, μ_{cs} (49). Thus, for the same sample CLS-25 we get

$$\langle \mu_{vir} \rangle = 3 \langle f_m(c) \mu_{cs} / c^2 \rangle \approx 17(1 \pm 0.28) M_{13}^{0.35} M_{\odot} / pc^2. \quad (51)$$

These results can be compared with recently published data by Babyk et al. (2012). For the sample CLS-30 of 30 clusters randomly selected from this survey we get

$$\langle \mu_{vir} \rangle \approx 13(1 \pm 0.11) M_{13}^{0.35} M_{\odot} / pc^2. \quad (52)$$

However in this survey all cluster characteristics are found with the popular assumption that $z_{cr} = z_{obs}$ what distorts their virial parameters, M_{vir} & R_{vir} , and makes impossible discussion of characteristics of the cluster cores. Prominent differences between scatters (51) and (52) are caused mainly by the impact of cluster description rather than by their physical properties.

The relatively small interval of observed cluster masses and the limited reliability and precision of the complex procedure of reconstruction of cluster characteristics (see, e.g., Bryan & Norman 1998; Pointecouteau et al. 2005; Pratt et al. 2009; Vikhlinin et al. 2009; Lloyd-Davies et al. 2011) strongly restricts the applicability of discussed scaling relations.

5 CONCLUSIONS

Abundant simulations show that the formation of virialized DM halos is a complex multistep process which begins as the anisotropic collapse in accordance with the Zel'dovich theory of gravitational instability (Zel'dovich 1970). During later stages the evolution of such objects is complicated and it goes through the stages of violent relaxation and merging. Non the less after a period of rapid evolution the main characteristics of the high density virialized DM halos become frozen and their properties are slowly changing owing to the accretion of diffuse matter and/or the evolution of their baryonic component.

The basic properties of the relaxed DM halos are determined by their global characteristics, namely, their mass, angular momentum and entropy generated in the course of violent relaxation of compressed matter. Basically the structure of such halos is similar to the structure of clusters of galaxies (see, e.g., Tasitsiomi et al. 2004; Nagai et al. 2007; Croston et al. 2008; Pratt et al., 2009, 2010; Arnaud et al. 2010; Kravtsov & Borgani 2012). In particular in these papers the generalized NFW model proposed in Zhao (1996) and Nagai et al. (2007) is discussed.

The basic properties of halos can be reproduced in the framework of the popular spherical model of halos formation. Such models have been discussed for many years (see, e.g., Peebles 1967; Zel'dovich & Novikov 1983; Fillmore & Goldreich 1984; Bryan & Norman 1998; Lithwick, Dalal 2011). However this model ignores many important features of the process of halos formation and is based on the assumption that during a short period of the spherical collapse at $z \approx z_{cr}$ the DM forms virialized halos with parameters which later vary slowly owing to the successive matter accretion (see, e.g., discussion in Bullock et al. 2001; Diemer et al. 2013).

In this paper we use the analytical description of the virialized spherical DM halo with the NFW density profile proposed in Klypin et al. (2011). Such approach allows us to formulate in Sec. 2 two parametric spherical model of virialized halos which is specified by the virial halo mass, M_{vir} , and redshift of formation z_{cr} . Of course this redshift is only some conventional characteristic of the mean density of virialized halos or other corresponding parameters. However, it can be used in order to roughly characterize the period of halos virialization what in turn allows to order the observed halos with respect to the (conventional) moment of formation. It also opens up the comparatively simple way to reveal correlations of thus introduced redshifts with the shape of the initial power spectrum.

5.1 Mass dependence of the redshift of formation of DM halos

These problems are discussed in Sec. 4 where we obtained the approximate relation between the virial mass of DM objects and their redshifts of formation. According to the commonly accepted hierarchical model of galaxy formation at high redshifts the formation of low mass galaxies dominates and the typical mass of formed galaxies successively increases with time. These expectations are illustrated by the expressions (32), (37) – (39). The high redshifts of formation of dSph and And galaxies correlate well with their low metal abundance and help us to reconstruct the history of the Local Group discussed for instance by Peebles (1995, 1996), Klypin et al. (2002, 2003).

Combining the resulting estimates (38) and (39) for mass dependence of the redshift of formation for both DM dominated observed dSph galaxies and clusters of galaxies we conclude that for these objects

$$\langle B^{-1}(z_{cr}) \rangle \approx 2.3(1 \pm 0.15)/M_{13}^{\beta}, \quad (53)$$

$$\beta \sim 0.1, \quad 10^5 M_{\odot} \leq M_{vir} \leq 10^{14} M_{\odot}.$$

With respect to the general theory of gravitational instability for the DM objects the expression (53) quantify

the mass dependence of the mean redshift of formation, $z_{cr}(M_{13})$, or correlation between these redshifts and the shape of the initial power spectrum of perturbations. Indeed according to the standard Λ CDM cosmology low mass objects (such as galaxies) are presumably formed earlier than more massive galaxies and clusters of galaxies and the expression (53) illustrate this statistical tendency.

Thus for the standard CDM – like power spectrum $p(k)$ (Bardeen et al. 1986) we have for the density perturbations (Klypin et al. 2011)

$$\sigma_m^2 = 4\pi \int_0^{\infty} p(k)W^2(kR)k^2 dk, \quad \sigma_m \propto M^{-0.1}, \quad (54)$$

for $10kpc \leq R \leq 10Mpc$, $10^5 \leq M/M_{\odot} \leq 10^{14}$. Here $W(kr)$ is the standard top-hat window function. Following the Press – Schechter approach (Press & Schechter 1974; Peebles 1974; Mantz et al. 2010) we can determine the redshift of objects formation from the condition

$$B(z_{cr})\sigma_m(M) \approx const, \quad B^{-1}(z_{cr}) \propto \sigma_m(M) \propto M^{-0.1}.$$

This result is consistent with (53) and confirms that the CDM-like power spectrum can be extended at least down to the scale of $\sim 10kpc$. However this approach does not allow us to obtain an independent estimate of the small scale amplitude of perturbations. More detailed comparison of the mass dependence of the redshift of formation of galaxies and clusters of galaxies requires much more precise estimates of observational parameters of both galaxies and clusters of galaxies.

For completeness it is interesting also to consider objects with intermediate masses $M_{vir} \sim 10^{10} M_{\odot} - 10^{12} M_{\odot}$. The virialized groups of galaxies and the far periphery of isolated galaxies can be used for such analysis if it is possible to confirm that they are dominated by DM and to estimate their virial characteristics. Perhaps it is simpler to estimate the correlation between the measured circular velocity $v_c^2 = GM_{vir}/R_{vir}$ and the virial radius R_{vir} . For $(1 + z_{cr}) \propto M^{-\beta}$ (53) we can expect that

$$v_c^2 = GM_{vir}/R_{vir} \propto R_{vir}^{\gamma}, \quad \gamma = (2 - 3\beta)/2(1 + \beta), \quad (55)$$

and $\gamma = 0.8$ for $\beta \approx 0.1$.

5.2 Formation of the first galaxies

It is quite interesting to compare the limits (28) with the observed properties of low mass galaxies (32 & 33). The first one restricts the virial masses of DM halos allowing for the rapid creation of metal free stars and the UV radiation. The second one considers the most probable masses of DM halos forming at the same redshifts as is suggested by observations of the dSph galaxies.

Such comparison is presented in Fig. 5 where the expected minimal masses of the DM halos with rapid star formation (Eqs. (28) and (56))

$$M_{vir} = [17.1/(1 + z_{cr})]^{10} 10^6 M_{\odot}, \quad (56)$$

are compared with the observed masses and redshift of formation for the dSph galaxies (points, stars and fit (57)):

$$M_{gal} = [17.6/(1 + z_{cr})]^{10.5} 10^6 M_{\odot}. \quad (57)$$

For 44 clusters of sample CLS-83 with $P_c \leq 70eV/cm^3$

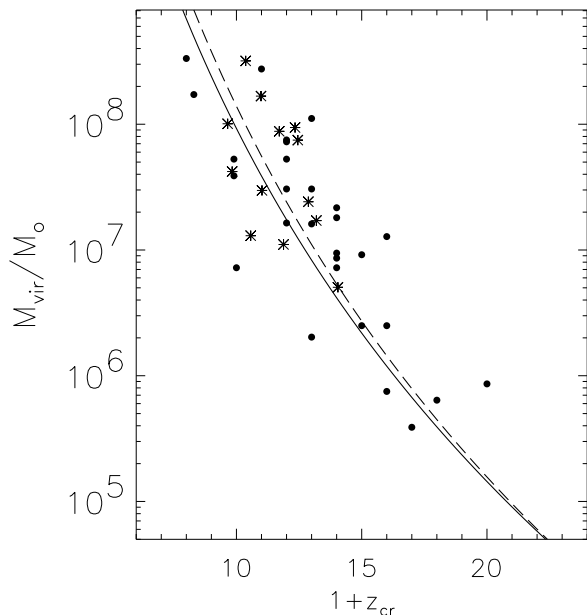


Figure 5. The observed masses of dSph (points) and And (stars) galaxies, M_{vir}/M_{\odot} , are plotted vs. their redshifts of formation, z_{cr} . Dashed line shows the fit (57). Solid line shows the redshift dependence of the minimal virial mass of DM halos with rapid formation of first stars (28, 56).

the correlation of the virial mass of halos and their redshift of formation is fitted by expression

$$M_{cls} = [17/(1+z_{cr})]^8 10^6 M_{\odot}, \quad (58)$$

and is plotted in Fig. 6. As is seen from (40) the cooling of baryonic component artificially decreases the estimate of virial mass M_{vir} and increases the estimate of redshift z_{cr} what enhances the scatter of points in Fig. 6. In spite of this the similarity of expressions (56) - (58) reflects the close link of all these objects formed with the joint power spectrum of initial perturbations. Weaker variation M_{cls} as a function of z_{cr} (58) as compared with (57) is naturally explained by weaker mass dependence of the amplitude $\sigma_m(M)$ for cluster masses.

The complex process of retrieval of considered characteristics of the dSph galaxies (see, e.g., Walker 2012) and the plausible impact of their prolonged evolution – such as the probable tidal striping – makes detailed discussion of the observed properties of such objects unreliable. In spite of this the comparison performed in Fig. 5 is interesting. First of all it confirms the probable formation of metal free galaxies with $M_{vir} \leq 10^9 M_{\odot}$ at redshifts $z \sim 20 - 8$ what agrees well with both other observations (see, e.g., Wyithe et al. 2013) and theoretical expectations discussed in Sec. 5.1.

On the other hand this Figure shows that the dSph galaxies are concentrated near the joint approximate boundary (28, 32). Such concentration indicates that the observed dSph galaxies can be really related with the earlier DM objects with various rate of star formation. Thus in objects disposed to the right of the demarcation lines (28, 32) the rapid star formation can be expected. In contrast in objects disposed to the left of these lines the star formation can be partly inhibited either by both the low ionization of the

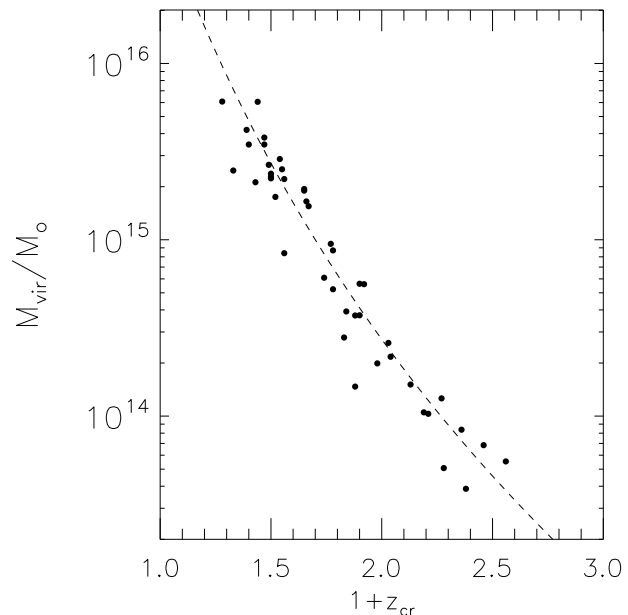


Figure 6. For 44 clusters of the sample CLS-83 with $P_c = n_c T_c \leq 70 \text{ eV/cm}^3$ the virial halo masses, M_{vir}/M_{\odot} , are plotted vs. their redshift formation, $1+z_{cr}$. Dashed line shows the fit (58).

compressed matter and by the impact of LW background. It can be later stimulated by an action of external factors such as, for example, ionizing UV radiation of external sources after dissipation of the LW background.

It is interesting also to compare other observed properties of these groups of dSph galaxies such as their metallicity and the possible populations of black holes.

These results show also that the most efficient star formation takes place in halos with $10^7 \leq M/M_{\odot} \leq 10^9$ (28) at redshifts $z \sim 13 - 8$ when probably the reionization actually occurs. This inference is consistent with observations of galaxies at redshifts $z \geq 7$ with $M \sim 3 \cdot 10^8 - 10^9 M_{\odot}$ (Ouchi et al. 2009; Schaerer & de Barros 2010; Gonzales et al. 2010, 2012; Oesch et al. 2013; Ellis et al. 2013). However, observations of Bouwens et al. (2011, 2012) indicate a possible more significant contribution of less massive galaxies.

All theoretical expectations can be essentially corrected by possible impact of the UV, LW and/or IR background (see, e.g. discussion in Loeb & Barkana 2001; Muñoz et al. 2009; Wolkott-Green & Haiman 2012 and references therein). As was noted in Sec. 3.5 the production of the UV background required for reionization by stars or other sources of radiation with the thermal spectrum is inevitably accompanied by formation of the corresponding LW background and deceleration of the process of star formation. In this case the UV radiation generated by matter accretion onto black holes with various masses can become dominant and can really determine the reionization. This verifies that such non thermal sources of the UV radiation can be considered as very promising ones and can be actually responsible for the reionization (see, e.g., Madau & Rees 2001; Reed 2005; Meiksin 2005, 2009; Madau 2007; Giallongo et al. 2012). Perhaps, the contribution of such sources can be confirmed by observations of tracks of He lines such as 304 Å and 584 Å shifted to the redshift of reionization.

5.3 The DM surface density of relaxed objects

If the redshift of formation of DM dominated objects can be directly linked with the power spectrum of density perturbations then both the central and virial surface densities of these objects, μ_{cs} & μ_{vir} , should depend upon the processes of violent relaxation of compressed matter and characterize this process. In particular, as it is seen from relations (14, 47), we can expect a weak mass dependence of the central surface density $\mu_{cs}(M_{vir})$ at galactic scale (45) but these expectations are distorted at clusters of galaxies scale (50). The virial surface density only weakly dependence on mass at both galactic and clusters of galaxies scales.

Both surface densities are closely linked with the DM density profile formed in the course of violent relaxation of the compressed matter and are determined by the action of the same factors. Non the less it can be expected that a weak mass dependence of the central surface density, μ_{cs} , can be observed across wide set of objects of galactic scales what will be an important additional evidence in favor of the standard shape of small scale initial power spectrum.

Acknowledgments

This paper was supported in part by the Russian Found of Fundamental Investigations grants Nr. 11-02-00244, and NS-2915.2012.2 and by the Polish Ministry of Science and Higher Education grant NN202-091839. AD thanks S.Pilipenko, B.Komberg and M. Sharina for useful comments. We wish to thank the anonymous referee for many valuable comments.

REFERENCES

Ade, P., et al. 2013, arXiv:1303.5076
 Arnaud, M., Pointecouteau, E., Pratt, G., 2005, A&A, 441, 893
 Arnaud, M., Pratt, G., Piffaretti, R., Böringer, H., Croston, J., Pointecouteau, E., 2010, A&A, 517, 92; arXiv:0910.1234
 Angulo, R., Springel, V., White, S.D.M., Jenkins, A., Baugh, C., Frenk, C., 2012, arXiv:1203.3216
 Babyk, I., Vavilova, I., Del Popolo, A., arXiv:1208.2424
 Bardeen J.M., Bond J.R., Kaiser N., & Szalay A., 1986, ApJ, 304, 15
 Barone-Nugent, R., Wyithe, J., Trenti, M., Treu, T., Oesch, P., Bradley, L., Schmidt, K., 2013, arXiv:1303.6109
 Besanson, R., van Dokkum, P., van de Sande, J., Franx, M., Leja, J., Kriek, M., 2013, arXiv:1309.6638
 Bhattacharya, S., Habib, S., Heitmann, K., Vikhlinin, A., 2013, ApJ, submit., arXiv:1112.5479
 Bouwens, R., et al., 2011, Nature, 469, 504
 Bouwens, R., et al., 2011, ApJ, 737, 33
 Bouwens, R., et al., 2012, ApJ, 752, L5
 Bouwens, R., et al., 2012, arXiv:1211.2230
 Branchesi, M., Gioia, I., Fanti, C., Fanti, R., 2007, A&A, 472, 739
 Bromm, V., and Yoshida, N., 2011, ARA&A, 49, 37
 Bryan, G., Norman, M., 1998, ApJ, 495, 80
 Bullock, J., Kolatt, T., Sigad, Y., Somerville, R., Kravtsov, A., Klypin, A., Primack, J., Dekel, A., 2001, MNRAS, 321, 559
 Burkert A., 1995, ApJ, 447, L25
 Ceverino, D., Klypin, A., Klimek, E., Trujillo-Gomez, S., Churchill, G., Primak, J., Dekel, A., 2013, arXiv:1307.0943
 Croston, J., et al., 2008, A&A, 487, 431
 Demiański, M., Doroshkevich, A., 1999, ApJ, 512, 527
 Demiański, M., Doroshkevich, A., 2004, A&A, 422, 423

Demiański, M., Doroshkevich, A., Pilipenko, S., Gottlöber, S., 2011, MNRAS, 414, 1813.
 Diemand, J., Kuhlen, M., Madau, P., 2007, ApJ, 667, 859
 Diemer, B., More, S., Kravtsov, A., 2013, arXiv:1207.0816
 Dijkstra, M., Haiman, Z., Loeb, A., 2004, ApJ, 613, 646
 Dolag, K., Bartelmann, M., Perrotta, F., Baccigalupi, C., Moscardini, L., Meneghetti, M., Torman, G., 2004, A&A, 416, 853
 Donato, F., Gentile, G., Salucci, P., Martins, C., Wilkinson, M., Gilmore, G., Grebel, E., Koch, A., Wyse, R., 2009, MNRAS, 397, 1169
 Doroshkevich A., Zel'dovich Ya., 1981, JETP, 80, 801
 Ellis, R., et al., 2013, arXiv:1211.6804
 Ettori, S., Tozzi, P., Borgani, S., Rosati, P., 2004, A&A, 417, 13
 Fan X. et al., 2004, AJ, 128, 515
 Fan X., Carilli C.L., Keating B., 2006, ARA&A, 44, 415
 Fillmore J.A., & Goldreich P., 1984, ApJ, 281, 1
 Foëx et al., 2013, A&A, in press, arXiv:1208.4026
 Furlanetto S., Peng Oh S., 2008, ApJ, 682, 14
 Gentile, G., Famaey, B., Zhao, H., Salucci, P., 2009, NATURE, 461, 627
 Giallongo E., Menci, N., Fiore, F., Castellano, M., Fontana, A., Grazian, A., Pentericci, L., 2012, arXiv:1206.2950
 Gonzalez V., Labbe, I., Bouwens, R., Illingworth, G., Franx, M., Kriek, M., Brammer, G., 2010, ApJ, 713, 115
 Gonzalez V., Bouwens, R., Labbe, I., Illingworth, G., Oesch, P., Franx, M., MaGee, D., 2012, ApJ, 755, 13
 Greif T., Johnson, J., Klessen, R., Bromm, V., 2008, MNRAS, 387, 1021
 Gurevich, A., Zybin, K., 1995, Phys.Usp., 38, 687
 Haiman, Z., 2010, arXiv:1007.4741
 Hogan, C.J., Anderson, S.F., Rugers M.H., 1997, AJ, 113, 1495
 Hutchings, R., Santoro, F., Thomas P., Couchman, H., 2002, MNRAS, 330, 927
 Hyde J., Bernardi, M., 2009, MNRAS, 396, 1171
 Jakobsen, P., Boksenberg A., Deharveng J.M., Greenfield P., Jędrzewski R., Paresce F., 1994, Nature, 370, 35
 Johnson, J., 2011, arXiv:1105.5701
 Kaviraj, S., et al., 2013, MNRAS, 428, 925
 Kelly, B., Vestergaard, M., Fan, X., Hopkins, P., Hernquist L., Siemiginowska, A., 2010, arXiv:1006.3561, ApJ, 719, 1315
 Klypin, A., Zhao, H., Somerville, R., 2002, ApJ, 573, 597
 Klypin, A., Hoffman, Y., Kravtsov, A., Gottlöber S., 2003, ApJ, 596, 19
 Klypin, A. Trujillo-Gomez, S., Primack, J., 2011, ApJ, 740, 102; arXiv:1002.3660
 Komatsu, E., et al. 2011, ApJS, 192, 18
 Kravtsov, A., Borgani, S., 2012, arXiv:2012.5556
 Laport, C., Walker, M., Penarrubia, J., 2013, MNRAS, 433, 54L
 Larson, D., et al. 2011, ApJS, 192, 16
 Lehnert M., et al. 2010, Nature, 467, 940
 Lithwick Y., Dalal N., 2011, ApJ, 734, 100L, arXiv:1010.3723;
 Lloyd-Davies, E., 2011, MNRAS, 418, 14
 Loeb, A., Barkana, R., 2001, ARA&A, 39, 19
 Ludlow, A. et al., 2013, MNRAS, in press, arXiv:1302.0288
 Madau P., Rees M., 2001, ApJ., 555, 9
 Madau P., 2007, "The Emission Line Universe", eds. J. Cepa and N. Sanchez, Cambridge University Press, arXiv:0706.0123
 Mancini, C., Matute, I., Cimatti, A., Daddi, E., Dickinson, M., Rodighiero, G., Bolzonella, M. Pozzetti, L., 2009, AA, 500, 705
 Mantz, A., Allen, S., Rapetti, D., Ebeling, H., 2010, MNRAS, 406, 1759
 McDonald, M., et al., 2013, ApJ, 774, 23
 Meiksin A., 2005, MNRAS, 356, 596
 Meiksin A., 2009, RvMP., 81, 1405
 Mosleh, M., Williams, R., Franx, M., Kriek, M., 2011, ApJ, 727, 5

- Moughan, B., Giles, P., Randall, S., Jones, C., Formen, W., 2011, arXiv:1108.1200
- Muñoz, J., Madau, P., Loeb, A., Diemand J., 2009, MNRAS, 400, 1593
- Nagai, D., Kravtsov, A., Vikhlinin A., 2007, ApJ, 668, 1
- Navarro J.F., Frenk C.S., & White S.D.M., 1995, MNRAS, 275, 720
- Navarro J.F., Frenk C.S., & White S.D.M., 1996, ApJ, 462, 563
- Navarro J.F., Frenk C.S., & White S.D.M., 1997, ApJ, 490, 493
- Oesch, P.A., et al., 2013, arXiv:1301.6162
- Ouchi, M., et al., 2009, ApJ, 706, 1136
- Peebles P.J.E., 1967, ApJ, 147, 859
- Peebles P.J.E., 1974, ApJ, 189, L51
- Peebles P.J.E., 1995, ApJ, 449, 52
- Peebles P.J.E., 1996, ApJ, 473, 42
- Penarrubia, J., Benson, A., Walker, M., Gilmore, G., McConnachie, A., Mayer, L., 2010, MNRAS, 406, 1290
- Piffaretti, R., Arnaud, M., Pratt, G., Pointecouteau, E., Melin, J., 2011, A&A, 534, 109.
- Pointecouteau, E., Arnaud, M., Pratt, G., 2005, A&A, 435, 1
- Prada, F., Klypin, A., Cuesta, A., Betancort-Rijo, J., Primack, J., 2011, arXiv:1104.5130
- Pratt, G., Arnaud, M., Pointecouteau, E., 2006, A&A, 446, 429
- Pratt, G., Croston, J., Arnaud, M., Böringer, H., 2009, A&A, 498, 361
- Pratt, G., et al., 2010, A&A, 511, A85
- Press, W., Schechter, P., 1974, ApJ, 187, 425
- Press, W., Rybicki, G., 1993, ApJ, 418, 585
- Reed D., Bower R., Frenk C., Gao L., Jenkins A., Theuns T., White S., 2005, MNRAS, 363, 393.
- Robertson B.E., Ellis R., Dunlop J., McLure R., Stark D., 2010, Nature, 468, 49
- Safrank-Shrader, C., Agarwal, M., Federrath, C., Dubey, A., Milosavljevic, M., Bromm, V., 2012, MNRAS, 426, 1159
- Salvadori, S., Tolstoy, E., Ferrara, A., Zharoubi, S., 2013, arXiv:1309.7058
- Salucci, P., Wilkinson, M., Walker, M., Gilmore G., Grebel, E., Koch, A., Martins, C., Wyse, R., 2012, MNRAS, 420, 2034 *
- Schaerer, D., Barros, S., 2010, A&A, 515, 15 *
- Shull, M., Harness, A., Trenti, M., Smith, B., 2011, arXiv:1108.3334
- Smette, A., Heap, S.R., Williger G.M., Tripp, T.M., Jenkins, E.B., Songaila A., 2002, ApJ, 564, 542
- Spano M., Marcelin, M., Amram, P., Carignan, C., Epinar, B., Hernandez, O., 2008, MNRAS, 383, 297
- Suhada, R., et al., 2012, A&A, 537, 39, 1076, arXiv:1111.0141
- Tasitsiomi, A., Kravtsov, A., Gottlöber, S., Klypin, A., 2004, ApJ, 607, 125
- Tollerud et al., 2012, ApJ, 752, 45
- Trenti, M., Stiavelli, M., Shull, M., 2009, ApJ, 700, 1672
- Trenti, M., Shull, M., 2010, ApJ, 712, 435
- Tumlinson, J., Venkatesan, A., Shull, M., 2004, ApJ, 612, 602
- Umemura, M., Loeb, A., Turner, E., ApJ, 419, 459
- Vestergaard, M., Osmer, P., 2009, ApJ, 699, 800
- Vikhlinin, A., Kravtsov, A., Forman, W., Jones, C., Markevitch, M., Murrey, S., Van Speybroeck, L., 2006, ApJ, 640, 691
- Vikhlinin, A., et al., 2009, ApJ, 692, 1033
- Visbal, E., Loeb, A., Hernquist, L., 2012, arXiv:1206.5852
- Walker, M., et al. 2009, ApJ., 704, 1274
- Walker, M. 2012, arXiv:1205.0311
- Wiklund, T., Dickinson, M., Ferguson, H., Giovalisco, M., Mobasher, B., Grogin, N., Panagia, N., 2008, ApJ, 676, 781
- Wise, J., & Abel, T., 2007, ApJ, 665, 899
- Wise, J., & Abel, T., 2008, ApJ, 685, 40
- Wolkott-Green, J., Haiman, Z., 2012, MNRAS, 425L, 51 arXiv:1206.1861
- Wyithe, J., Stuart, B., & Loeb, A., 2013, MNRAS, 428, 2741
- Wyithe, J., Loeb, A., Oesch, P., 2013, arXiv:1308.2030
- Zel'dovich Ya.B., 1970, A&A, 5, 84
- Zel'dovich Ya.B., Novikov I.D., 1983, Structure and evolution of the Universe, University of Chicago Press.
- Zhang, Y., Böringer, H., Finoguenov, A., Ikebe, Y., Matsushita, K., Schueker, P., Guzzo, L., Collins, C., 2006, A&A, 456, 55
- Zhao, H., 1996, MNRAS, 278, 488